Dyes and Pigments 128 (2016) 304–313

Contents lists available at ScienceDirect

Dyes and Pigments

journal homepage: www.elsevier.com/locate/dyepig

Two novel phenylethene-carbazole derivatives containing dimesitylboron groups: Aggregation-induced emission and electroluminescence properties

Heping Shi [a, d, *], Min Li [a], Dehua Xin [a], Li Fang [a], Jesse Roose [b], Huiren Peng [c], Shuming Chen [c, **], Ben Zhong Tang [b, ***]

[a] School of Chemistry and Chemical Engineering, Shanxi University, Taiyuan 030006, PR China
[b] Department of Chemistry, Institute for Advanced Study, Division of Biomedical Engineering, Division of Life Science, State Key Laboratory of Molecular Neuroscience, Institute of Molecular Functional Materials, The Hong Kong University of Science and Technology, Clear Water Bay, Kowloon, Hong Kong, China
[c] Department of Electrical and Electronic Engineering, South University of Science and Technology of China, Shenzhen, Guangdong 518055, PR China
[d] State Key Laboratory of Structural Chemistry, Fujian Institute of Research on the Structure of Matter, Chinese Academy of Sciences, Fu Zhou, Fujian 350002, PR China

ARTICLE INFO

Article history:
Received 14 December 2015
Received in revised form
25 January 2016
Accepted 28 January 2016
Available online 6 February 2016

Keywords:
Phenylethene
Carbazole
Dimesitylboron
Synthesis
Aggregation-induced emission
Electroluminescence

ABSTRACT

Two novel phenylethene-carbazole derivatives containing dimesitylboron groups, 3-(dimesitylboryl)-9-ethyl-6-(1,2,2-triphenylvinyl)-9*H*-carbazole and 1,2-bis(6-(dimesitylboryl)-9-ethyl-9*H*-carbazol-3-yl)-1,2-diphenylethene are presented. The foregoing mono- and bis-carbazole containing compounds combine the aggregation-induced emission properties of phenylethene and the hole and electron transporting properties of carbazole and dimesitylboron substituents respectively. An extensive investigation of their optical and electrical properties reveals that these aggregation-induced emission active scaffolds exhibit excellent thermal stability (T_d up to 254 °C) with high electrochemical stability. Compared to our previous systems, the OLED device using the mono-carbazole derivative as a sky-blue emitter shows improved parameters such as the maximum luminance and maximum luminance efficiency of 13,930 cd m^{-2} and 4.74 cd A^{-1}, respectively. The device based on the blue–green emitting bis-carbazole derivative features equally high maximum luminance and maximum luminance efficiency of 15,780 cd m^{-2} and 6.90 cd A^{-1}, respectively.

1. Introduction

Over the past decades, considerable interest has been attracted to the research field of organic light-emitting diodes (OLEDs) due to their wide-ranging applications in full-color flat-panel displays and solid state lighting [1–4]. To obtain high-performance OLEDs, scientists have prepared a wide variety of efficient emissive materials with excellent properties. Up to now, red- and green-emitters have shown outstanding performance in terms of luminance and efficiency [5,6]. However, it is still a challenge to develop blue luminogens with good performance [7–9] due to their intrinsic wide bandgap which makes it very difficult to inject charges into the blue emitters [10–18]. Meanwhile, most of blue-emitters show poor performance in practical applications when they are fabricated as thin solid films since they suffer from the notorious aggregation-caused quenching (ACQ) effect [19,20]. The ACQ effect has become a thorny problem for the development of efficient OLEDs. Therefore, the preparation of blue-emitting materials with high efficiency in the aggregate phase becomes particularly important [19,21,22].

In 2001, Tang and co-workers discovered that a series of propeller-like luminogens being practically non-fluorescent in solutions became highly emissive upon aggregate formation or in the solid crystalline state [23]. This phenomenon known as aggregation-induced emission (AIE) constitutes the exact opposite of the ACQ effect. They further elaborated that the restriction of intramolecular rotation (RIR), more general, the restriction of

* Corresponding author. School of Chemistry and Chemical Engineering, Shanxi University, Taiyuan 030006, PR China.
** Corresponding author.
*** Corresponding author.
E-mail addresses: hepingshi@sxu.edu.cn (H. Shi), chen.sm@sustc.edu.cn (S. Chen), tangbenz@ust.hk (B.Z. Tang).

http://dx.doi.org/10.1016/j.dyepig.2016.01.028
0143-7208/

intramolecular motion (RIM) is the predominant mechanism causing the AIE effect [24–28]. The discovery of this phenomenon opened a concise avenue to solve the ACQ problem of luminescent materials and to achieve high-performance OLEDs without the need of using dopants or other adjuvants.

Nowadays, many AIE luminogens (AIEgens), such as derivatives of silole [29–32], tetraphenylethene (TPE) [33–39], distyrylanthracene (DSA) [40,41], triphenylethene (TrPE) [42–45], and tetraphenyl-1,4-butadiene (TPBD) [46,47], have been reported by Tang and other groups. Among these typical AIE materials, TrPE is considered as one of the ideal candidates for blue-OLED applications since with its twisted configuration of the three phenyl rings it possesses a low conjugation compared to TPE, which renders most TrPE derivatives as blue emitters. Furthermore, it has been demonstrated by Tang and co-workers that its emission is much bluer than TPE with an as large as 25 nm hypsochromatic shift of the emission maximum [48]. In addition, many different functional groups can be introduced into the TrPE skeleton, offering a versatile approach to design the ideal luminogen for the respective application [42,49]. Due to these features, several TrPE-based derivatives have been synthesized. Chi and co-workers synthesized and characterized a series of AIE-active triphenylethylene-carbazole derivatives with good thermal properties and blue light emission capabilities [42,50–53]. In line with that report, Tang and co-workers designed and synthesized three luminogens from TrPE, carbazole and triphenylamine (TPA) building blocks exhibiting AIE behavior. Multilayer OLEDs fabricated by utilizing these luminogens exhibited blue light with high luminance and current efficiency [54]. Later, they utilized TrPE as a building block for constructing an AIE-active deep blue emitter, BTPE-PI (Chart 1), which was thermally stable with balanced carrier injection properties. The non-doped deep blue OLED fabricated by using BTPE-PI as emitting layer showed a very high external quantum efficiency of 4.4% with only a small roll-off current [48]. These research results inspire us to further successfully exploit the advantageous properties of TrPE derivatives to furnish blue electroluminescence materials.

Similarly to TrPE, diphenylethene (DPE), commonly known as stilbene, provides a good platform to substitute the olefinic protons with two rather than one available side. Tang and his group synthesized a series of new AIE materials by replacing of phenyl ring(s) in tetraphenylethene with naphthalene ring(s), among which DNDPE (Chart 1) was one of DPE derivatives and showed blue emission. Compared to TPE, the thermal and electroluminescence properties of DNDPE turned out to be more advantageous [55]. This suggests that DPE equipped with extended aromatic structures can be utilized to construct novel AIE-active emitters. Carbazole forms the basis of a class of well-known hole-transporting materials. Recently, it has been one of the scaffolds of choice to design new luminescent molecules in combination with AIE-active molecules to overcome its own ACQ effect in the condensed state [33,51,56–58]. To the best of our knowledge, Liu et al. were the first researchers to report a carbazole-containing DPE derivative with typical AIE characteristics, which formed highly blue emissive crystal fibers, and enjoyed enhanced optical and electronic properties [59]. Their results demonstrated the great potential of carbazole-substituted ethene derivatives as optoelectronic materials. On the other hand, dimesitylboron moieties have been widely used as electron-acceptor units to construct electroluminescent materials for the advantage of optoelectronic properties. Besides, the bulk steric effect and twisted conformation of dimesitylboron could also prevent ACQ, resulting in highly efficient solid-state emitting [60,61].

In line with the above-mentioned considerations and facts, we herein report the synthesis of two new phenylethylene-carbazole derivatives, 3-(dimesitylboryl)-9-ethyl-6-(1,2,2-triphenylvinyl)-9*H*-carbazole (DETPCZ) and 1,2-bis(6-(dimesitylboryl)-9-ethyl-9*H*-carbazol-3-yl)-1,2-diphenylethene (DECZDPE). DETPCZ was obtained by fusing TrPE and one carbazole moiety into one system with one dimesitylboron group attached to the carbazole part. DECZDPE was synthesized using a similar design strategy that was based on a DPE having two carbazole substituents as a backbone and two dimesitylboron groups attached on the periphery. Both synthetic routes are presented in Scheme 1. To the best of our knowledge, these compounds have never been reported before. Both molecules were characterized by elemental analysis, ^{1}H NMR, ^{13}C NMR, IR and MS. In addition, we report their thermal, electrochemical, and photophysical properties. Our work particularly highlights the advanced properties regarding their thermal stability, strong solid state emission in combination with the AIE-behavior, and the enhanced electroluminescence (EL) performance.

2. Experimental section

2.1. Materials and instrumentation

THF was distilled from a sodium benzophenone mixture under dry nitrogen immediately prior to use. All the chemicals and reagents were purchased from commercial sources without further

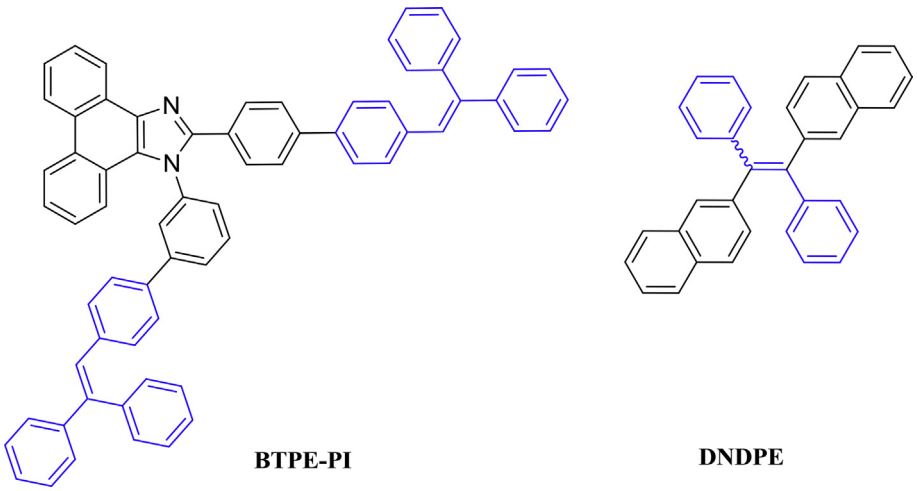

Chart 1. Chemical structures of **BTPE-PI** and **DNDPE**.

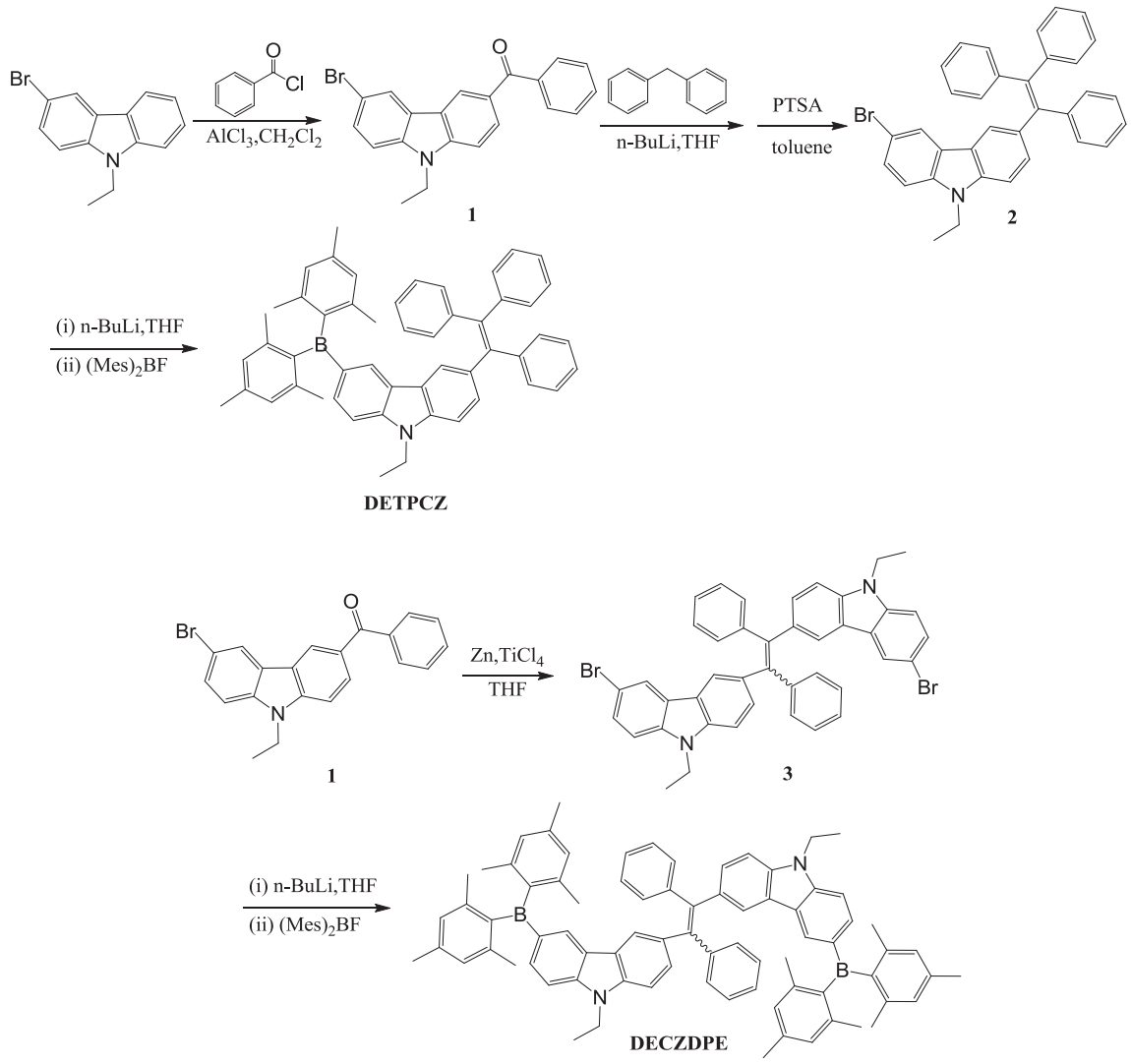

Scheme 1. Synthetic routes to **DETPCZ** and **DECZDPE**.

purification unless otherwise stated. All the reactions were carried out under an inert nitrogen atmosphere. ^{1}H and ^{13}C NMR spectra were recorded on a Bruker 600 MHz spectrometer in deuterated chloroform. High-resolution mass spectra (HRMS) were recorded on an Autoflex III (MALDI-TOF-MS). Mass Spectrometer System operating in a MALDI-TOF mode. Elemental analyses were performed on an Element Analysis System. Infrared (IR) spectra were obtained using Perkin Elmer Spectrum GX II FT-IR System. The spectra of the solid compounds were recorded in the form of KBr pellets. UV spectra were recorded on a Shimadzu UV-2450 absorption spectrophotometer. Fluorescence measurements were conducted on a Shimadzu RF-5301PC fluorescence spectrometer. Thermogravimetric analysis (TGA) was carried out on a TA Instruments TGA 2050 thermogravimetric analyzer under nitrogen at a heating rate of 10 °C min^{-1} from room temperature to 500 °C. Differential scanning calorimetry (DSC) was performed using a Q2000 DSC differential scanning calorimeter under a N_2 atmosphere. Cyclic voltammetry was taken on a CHI-600C electrochemical analyzer. The measurements were determined using a conventional three-electrode configuration consisting of a glassy carbon working electrode, a platinum-disk auxiliary electrode and an Ag/AgCl reference electrode. And the scan rate was 10 mV/s. The fluorescence quantum yield was acquired using quinine sulfate as the reference (excited at 350 nm). All measurements were conducted at room temperature.

2.2. Device fabrication and testing

The multilayer OLEDs were fabricated using the vacuum-deposition method. Organic layers were fabricated by high-vacuum (5×10^{-4} Pa) thermal evaporation onto a glass (3 cm × 3 cm) substrate precoated with an ITO layer. Dipyrazinoquinoxaline-2,3,6,7,10,11-hexacarbonitrile (HATCN), *N*,*N*-bis(-naphthalene)-*N*,*N*-bis(phenyl)benzidine (NPB), DETPCZ or DECZDPE, and 1,3,5-tri(1-phenyl-1*H*-benzo[*d*]imidazol-2-yl) phenyl (TPBI) served as hole injection, hole-transporting, light-emitting and electron-transporting layers, respectively. Lithium fluoride (LiF) capped with aluminum (Al) was used as the cathode. All organic layers were sequentially deposited. Thermal deposition rates for organic materials, LiF and Al were 0.5 A s^{-1}, 0.5 A s^{-1} and 1 A s^{-1}, respectively. The light-emitting area of the devices was 9.0 mm^2. The EL spectra were recorded on a Hitachi MPF-4 fluorescence spectrometer. The current density-voltage characteristics of OLEDs were measured on a Keithley 2400 Source Meter. The current density–voltage–luminance curves were performed with a 3645 DC power supply combined with a 1980A spot photometer

simultaneously. All measurements were carried out at room temperature.

2.3. Synthesis

2.3.1. Synthesis of (6-bromo-9-ethyl-9H-carbazol-3-yl)(phenyl) methanone (**1**)

A stirred mixture of 3-bromo-9-ethyl-9*H*-carbazole (3.57 g, 13.03 mmol) and benzoyl chloride (2.19 g, 15.64 mmol) in CH_2Cl_2 (60 mL) was treated by slow addition of aluminum chloride (1.82 g, 13.67 mmol) under an atmosphere of nitrogen. The mixture was heated for 6 h at 40 °C. After cooling to room temperature, cold water (200 mL) was added to quench the reaction and the mixture was then extracted with CH_2Cl_2 (3 × 50 mL). The organic layer was washed with water and dried over magnesium sulfate. The crude product was purified by silica-gel chromatography ($R_f = 0.2$, with dichloromethane: petroleum ether 1:2 as eluent) to give **1** as a white solid (81%, 4.0 g). m.p. = 123–125 °C. IR (KBr), ν/cm^{-1}: 3060, 2974, 2930, 1643, 1618, 1587, 1481, 1446, 1386, 1347, 1326, 1305, 1284, 1274, 1259, 1235, 1154, 1136, 1126, 957, 788, 739, 715, 631. ^{1}H NMR (600 MHz, $CDCl_3$), δ (ppm): 8.55 (s, 1H), 8.23 (d, J = 1.34 Hz, 1H), 8.09 (d, J = 10.14 Hz, 1H), 7.86 (d, J = 7.08 Hz, 2H), 7.62–7.60 (m, 2H), 7.55 (m, 2H), 7.48 (d, J = 8.41 Hz, 1H), 7.35 (d, J = 8.61 Hz, 1H), 4.42–4.40 (m, 2H), and 1.50–1.47 (t, J = 14.58 Hz, 3H). ^{13}C NMR (600 MHz, $CDCl_3$), δ (ppm): 196.80, 143.06, 139.64, 139.15, 132.20, 130.25, 129.51, 129.30, 128.63, 125.29, 124.74, 123.90, 121.79, 113.18, 110.82, 108.81, 38.42, 14.19, 1.41. MS (MALDI-TOF): Calcd for $C_{21}H_{16}BrNO$, 378.0400; found, 378.0400. Anal. calcd for $C_{21}H_{16}BrNO$: C 66.68%, H 4.26% and N 3.70%. Found: C 66.66%, H 4.23%, and N 3.72%.

2.3.2. Synthesis of 3-bromo-9-ethyl-6-(1,2,2-triphenylvinyl)-9H-carbazole (**2**)

Under a N_2 atmosphere, a solution of diphenylmethane (1.06 mL, 6.4 mmol) in dry THF (40 mL) was treated dropwise with 4.0 mL *n*-butyllithium (1.6 M in hexane, 4.0 mL, 6.4 mmol) at 0 °C. The resulting orange–red mixture was stirred for 1.5 h at 0 °C and subsequently slowly transferred to a solution of **1** (2.0 g, 5.3 mmol) in THF (40 mL) at 0 °C. The mixture was allowed to warm to room temperature and stirring was continued for 18 h. The reaction was quenched by adding an aqueous solution of ammonium chloride, after which the organic layer was extracted with CH_2Cl_2 (3 × 50 mL). The combined organic phase was dried over magnesium sulfate, evaporated in vacuo, then dissolved in toluene (80 mL) and heated to reflux in the presence of *p*-toluenesulfonic acid (1.5 g, 8 mmol) for 6 h. After being cooled to room temperature, the resulting mixture was evaporated, washed with an aqueous sodium bicarbonate solution, extracted with CH_2Cl_2, and dried over anhydrous magnesium sulfate. After solvent evaporation, the crude product **2** was purified by silica gel column chromatography ($R_f = 0.3$, with dichloromethane: petroleum ether 1:12 as eluent). Yellow–green solid; yield 54% (1.5 g). m.p. = 235–237 °C. IR (KBr), ν/cm^{-1}: 3074, 3052, 3023, 2966, 1625, 1596, 1480, 1445, 1377, 1348, 1292, 1231, 1150, 1131, 812, 796, 764, 748, 701. ^{1}H NMR (600 MHz, $CDCl_3$), δ (ppm): 7.95 (d, J = 1.25 Hz, 1H), 7.67 (s, 1H), 7.47–7.45 (m, 1H), 7.21–7.16 (m, 2H), 7.10–7.02 (m, 16H), 4.25–4.22 (m, 2H), and 1.38–1.36 (t, J = 14.04 Hz, 3H). ^{13}C NMR (600 MHz, $CDCl_3$), δ (ppm): 144.76, 144.54, 144.52, 141.75, 140.64, 139.34, 139.16, 135.46, 131.91, 131.87, 131.83, 130.72, 128.44, 128.09, 128.03, 126.79, 126.62, 126.59, 125.11, 123.91, 123.49, 121.84, 111.90, 110.23, 108.15, 38.09, 14.20. MS (MALDI-TOF): Calcd for $C_{34}H_{26}BrN$, 529.2001; found, 529.2001. Anal. calcd for $C_{34}H_{26}BrN$: C 77.27%, H 4.96% and N 2.65%. Found: C 77.24%, H 4.93%, and N 2.67%.

2.3.3. Synthesis of 1,2-bis(6-bromo-9-ethyl-9H-carbazol-3-yl)-1,2-diphenylethene (**3**)

A 250 mL flask equipped with a stirrer was charged with zinc powder (2.0 g, 30.7 mmol) and THF (150 mL). $TiCl_4$ (1.5 mL, 13.8 mmol) was slowly added by a syringe at −78 °C under an atmosphere of nitrogen. The mixture was allowed to warm to room temperature and was heated to reflux for 4 h. Subsequently, **1** (1.5 g, 3.9 mmol) in THF (50 mL) was added at room temperature and the resulting mixture heated at 83 °C for 18 h. The reaction was quenched with a 10% K_2CO_3 aqueous solution and extracted with dichloromethane (3 × 50 mL). The combined organic phases were concentrated in vacuo and purified by silica-gel chromatography ($R_f = 0.3$, with dichloromethane: petroleum ether 1:6 as eluent) to give a yellow–green solid (0.85 g, 59%). m.p. = 294–296 °C. IR (KBr), ν/cm^{-1}: 3057, 2972, 1627, 1593, 1480, 1440, 1380, 1345, 1316, 1292, 1269, 1229, 1155, 1129, 878, 804, 794, 701. ^{1}H NMR (600 MHz, $CDCl_3$), δ (ppm): 7.96–7.92 (m, 2H), 7.72 (s, 2H), 7.46–7.42 (m, 2H), 7.23–7.16 (m, 4H), 7.12 (s, 9H), 7.07–7.03 (m, 3H), 4.27–4.18 (m, 4H), and 1.40–1.32 (m, 6H). ^{13}C NMR (600 MHz, $CDCl_3$), δ (ppm): 145.16, 141.05, 139.20, 139.15, 139.11, 135.91, 132.03, 131.98, 130.97, 130.83, 128.38, 128.31, 128.07, 128.01, 126.59, 126.55, 125.10, 123.91, 123.51, 121.88, 111.75, 110.17, 108.23, 108.14, 38.06, 30.09, 14.19, 14.13. MS (MALDI-TOF): Calcd for $C_{42}H_{32}Br_2N_2$, 724.3001; found, 724.3001. Anal. calcd for $C_{42}H_{32}Br_2N_2$: C 69.62%, H 4.45% and N 3.87%. Found: C 69.60%, H 4.43%, and N 3.90%.

2.3.4. Synthesis of 3-(dimesitylboryl)-9-ethyl-6-(1,2,2-triphenylvinyl)-9H-carbazole (**DETPCZ**)

A solution of **2** (0.7 g, 1.33 mmol) in dry THF (60 mL) was treated with a *n*-butyllithium solution (1.6 M in hexane, 1.66 mL, 2.65 mmol) at −78 °C under nitrogen. The resulting mixture was stirred at room temperature for 5 h followed by the slow addition of dimesitylboron fluoride (0.79 g, 3.0 mmol) after being cooled to −78 °C again, after which the mixture was warmed to room temperature and stirred for 24 h. The reaction was quenched with ice water (200 mL). The organic layer was extracted with dichloromethane (3 × 50 mL) and dried over anhydrous $MgSO_4$. After solvent evaporation, the residue was purified by silica gel column chromatography ($R_f = 0.2$, with dichloromethane: petroleum ether 1:10 as eluent). A yellow–green solid of **DETPCZ** was obtained (0.3 g, 33%). m.p. = 158–160 °C. IR (KBr), ν/cm^{-1}: 3058, 3017, 2977, 2915, 1607, 1591, 1480, 1445, 1380, 1348, 1287, 1232, 1213, 1168, 1152, 1129, 1028, 844, 807, 701. ^{1}H NMR (600 MHz, $CDCl_3$), δ (ppm): 8.07 (s, 1H), 7.70 (s, 1H), 7.61–7.59 (d, J = 8.41 Hz, 1H), 7.12–7.04 (m, 18H), 6.83 (s, 4H), 4.29–4.28 (m, 2H), 2.32 (s, 6H), 2.01 (s, 12H), 1.44–1.43 (t, J = 13.76 Hz, 3H). ^{13}C NMR (600 MHz, $CDCl_3$), δ (ppm): 139.50, 139.44, 138.30, 136.80, 136.13, 135.53, 134.20, 133.18, 130.61, 130.51, 126.78, 126.70, 126.68, 125.95, 124.94, 123.32, 122.88, 122.85, 121.61, 121.41, 121.30, 119.02, 118.45, 118.23, 103.00, 32.99, 22.17, 18.87, 16.48, 9.19. MS (MALDI-TOF): Calcd for $C_{52}H_{48}BN$, 697.3900; found, 697.3900. Anal. calcd for $C_{52}H_{48}BN$: C 89.51%, H 6.93% and N 2.01%. Found: C 89.57%, H 7.01%, and N 1.99%.

2.3.5. Synthesis of 1,2-bis(6-(dimesitylboryl)-9-ethyl-9H-carbazol-3-yl)-1,2-diphenylethene (**DECZDPE**)

DECZDPE was prepared from **3** (0.635 g, 0.88 mmol), *n*-butyllithium (2.2 mL, 3.51 mmol), and dimesitylboron fluoride (1.03 g, 3.86 mmol) in dry THF (80 mL). The procedures were similar to those for the synthesis of **DETPCZ**. ($R_f = 0.2$, with dichloromethane: petroleum ether 1:12 as eluent). Yellow–green solid; yield 33% (0.3 g). m.p. = 197–199 °C. IR (KBr), ν/cm^{-1}: 3052, 3023, 2972, 2920, 1607, 1591, 1482, 1443, 1380, 1348, 1290, 1229, 1216, 1152, 1126, 844, 804, 701. ^{1}H NMR (600 MHz, $CDCl_3$), δ (ppm): 8.14–8.08 (m, 2H), 7.77–7.72 (m, 2H), 7.61–7.57 (m, 2H), 7.24–7.20 (m, 3H), 7.12–7.08 (m, 9H), 7.03–7.02 (m, 4H), 6.83–6.81 (m, 8H), 4.29–4.22 (m, 4H),

2.31–2.26 (m, 12H), 2.02–1.94 (m, 24H), 1.39–1.32 (m, 6H). ^{13}C NMR (600 MHz, $CDCl_3$), δ (ppm): 144.77, 144.72, 143.05, 142.98, 142.26, 141.11, 140.89, 140.15, 138.84, 138.77, 138.62, 137.97, 137.91, 136.12, 135.78, 135.32, 135.27, 131.72, 131.66, 131.62, 130.76, 130.66, 130.38, 129.86, 128.08, 127.58, 126.15, 126.02, 123.81, 123.55, 123.48, 123.29, 123.24, 123.05, 122.46, 120.42, 118.64, 108.39, 108.33, 107.78, 107.74, 107.50, 53.45, 37.74, 37.67, 37.57, 37.51, 29.73, 26.94, 23.64, 21.24, 13.96, 13.89. MS (MALDI-TOF): Calcd for $C_{78}H_{76}B_2N_2$, 1062.6288; found, 1062.6588. Anal. calcd for $C_{78}H_{76}B_2N_2$: C 88.13%, H 7.21% and N 2.64%. Found: C 88.18%, H 7.26%, and N 2.68%.

3. Results and discussion

3.1. Synthesis

As shown in Scheme 1, both of the two target compounds, DETPCZ and DECZDPE, were obtained using a straight forward multi-step synthetic route. In the first step, compound **1** was synthesized via an $AlCl_3$-catalyzed Friedel–Crafts acylation of commercially available 3-bromo-9-ethyl-9*H*-carbazole with benzoyl chloride. The acylated carbazole derivative **1** was then treated with lithiated diphenylmethane, and subsequently dehydrated under acidic catalysis yielding compound **2** in good yield. To furnish the bis-substituted scaffold DECZPE, compound **1** was dimerized in a McMurry cross-coupling reaction affording compound **3**. Ultimately, DETPCZ and DECZDPE were obtained from **2** and **3**, respectively, via lithiation with *n*-butyllithium and subsequent substitution with dimesitylboron fluoride. All the intermediate and final products were fully purified and characterized, and the result data satisfactorily corresponded to the expected molecular structures. The detailed synthetic routes and structure characterization data of infrared spectroscopy, ^{1}H and ^{13}C nuclear magnetic resonance spectroscopy, mass spectrometry, and elemental analysis are presented in Experimental section.

3.2. Thermal properties

The thermal properties of DETPCZ and DECZDPE were investigated by thermogravimetric analysis (TGA) and differential scanning calorimetry (DSC) under a nitrogen atmosphere at a heating rate of 10 °C min^{-1}. As displayed in Fig. S1a and b (ESI†), the decomposition temperatures (T_d based on 5% weight loss) of DETPCZ and DECZDPE determined from the TGA curves are 254 °C and 173 °C, respectively. DSC analysis reveals that the glass transition temperatures (T_g) of both compounds amount to 88 °C (Fig. S2a and b†). These data are summarized in Table 1. The reasonably high T_d and T_g of DETPCZ and DECZDPE can be ascribed to their large molecular mass, the rigid carbazole moieties, and the non-planar phenylethene cores and dimesitylboron peripheries. These data indicate that the two compounds have excellent thermal stability which is beneficial for the lifetimes of OLED devices.

3.3. Theoretical calculations

To gain insight into the excitation and emission properties at the molecular level, density functional theory (DFT) computation at the B3LYP/6-31G(d,p) level were carried out by using Gaussian 03 software [62–65]. The optimized geometries of DETPCZ and DECZDPE in the ground state in combination with electron distributions of the highest occupied molecular orbital (HOMO) and the lowest unoccupied molecular orbital (LUMO) are shown in Fig. 1. The phenylethene unit is twisted from the plane of the carbazole and the peripheral dimesitylboron unit(s) in both molecules, which prevents emission quenching caused by unfavorable π–π stacking interactions. As shown in Fig. 1, the HOMO of DETPCZ is dominated by the orbitals from the phenylethene-carbazole core. The electron cloud of the LUMO, however, is mainly located on the carbazole moiety and the dimesitylboron unit. The distributions of the HOMO and the LUMO of DECZDPE are similar to those of DETPCZ, respectively. The energy levels of DETPCZ and DECZDPE partly overlap, which may lead to intramolecular charge transfer (ICT) effects. Table 1 summarizes the calculated HOMO and LUMO energy levels. With HOMO/LUMO energies of −5.06 and −1.39 eV for DETPCZ and −4.89 and −1.37 eV for DECZDPE, the HOMO-LUMO energy gaps amount to 3.67 eV and 3.52 eV, respectively. Compared to the HOMO–LUMO energy gaps obtained experimentally from the UV–vis absorption spectra, the theoretical HOMO–LUMO energy gaps of DETPCZ and DECZDPE are relatively larger.

3.4. Photophysical properties

DETPCZ and DECZDPE possess good solubility in common organic solvents, such as dichloromethane, chloroform, and tetrahydrofuran (THF), but both are insoluble in water. Fig. S3a and b (ESI†) show the absorption spectra of DETPCZ and DECZDPE in various solvents (1.0×10^{-5} M), respectively. The absorption spectra data are summarized in Table 1. DETPCZ exhibits two major absorption bands at 300–340 nm and 340–375 nm, respectively (Fig. S3a†). The absorption peak maximum (λ_{abs}) of 319 nm corresponds to the π–π^* electronic transition of the phenylethene-carbazole skeleton and λ_{abs} of 363 nm is attributed to intramolecular charge transfer (ICT) from the phenylethene-carbazole core to dimesitylboron terminal groups. The absorption spectra of DECZDPE are similar to those of DETPCZ in various solvents. The optical energy bandgap of DETPCZ calculated from the absorption band edge of the absorption spectrum is approximately 2.92 eV, while that of DECZDPE is approximately 2.87 eV.

Table 1
Physical properties of **DETPCZ** and **DECZDPE**.

Compound	λ_{abs}[a] (nm)	λ_{em}[b] (nm)	λ_{em}[c] (nm)	T_d[d] (°C)	T_g[d] (°C)	HOMO/LUMO[e] (eV)	E_g[f] (eV)	HOMO/LUMO[g] (eV)	E_g[g] (eV)
DETPCZ	319 363	487	481	254	88	−4.90/−1.98	2.92	−5.06/−1.39	3.67
DECZDPE	321 364	500	498	173	88	−5.38/−2.51	2.87	−4.89/−1.37	3.52

[a] Measured in THF.
[b] Measured in THF + H_2O(1:9).
[c] Measured in film.
[d] Obtained from TGA and DSC.
[e] Obtained from CV in CH_3CN/n-Bu_4NClO_4 and estimated from HOMO = −(E_{ox} + 4.40); LUMO = HOMO + E_g.
[f] Calculated from the absorption edge, $E_g = 1240/\lambda_{onset}$.
[g] Obtained from DFT calculations.

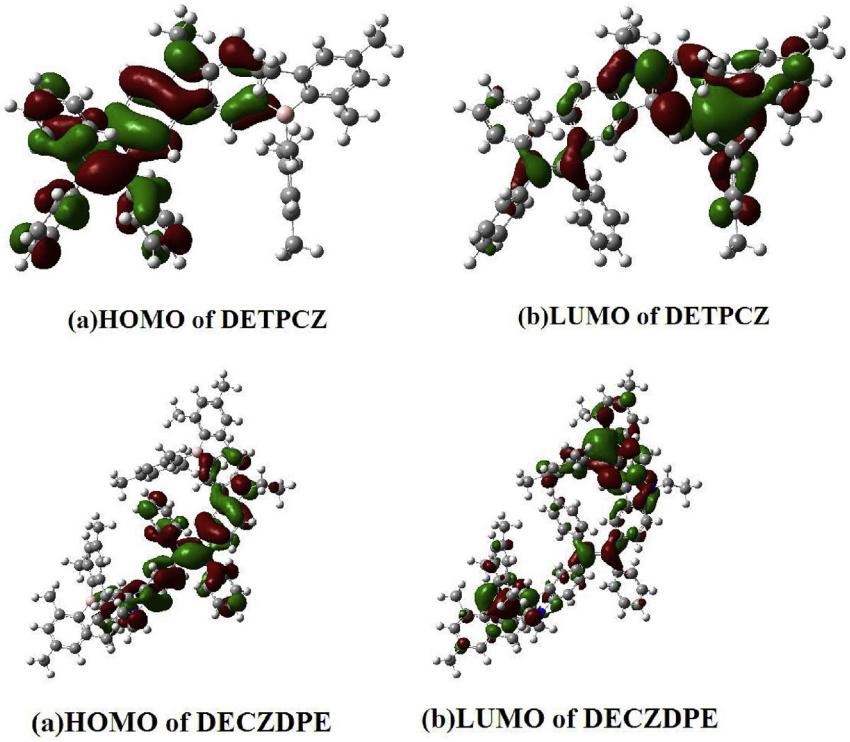

Fig. 1. **HOMO** and **LUMO** diagrams of **DETPCZ** and **DECZDPE**.

The fluorescence spectra of DECZDPE in various solvents (1.0×10^{-5} M) are shown in Fig. S4 (ESI†). DETPCZ exhibits no discernible fluorescence when dissolved in good solvents, and thus the fluorescence spectra of it were not measured. As depicted in Fig. S4†, the emission peak maximum (λ_{em}) exhibits a red-shift of 59 nm ranging from 388 nm (in hexane) to 447 nm (in DMSO) while the emission peak at 515 nm (in hexane) simultaneously vanishes with the increasing polarity of the solvents, which has been assigned to the intramolecular charge transfer (ICT) from the diphenylethene-carbazole core to the dimesitylboron groups in the excited state. The solid emission spectra of DETPCZ and DECZDPE were obtained by measuring their films displayed in Fig. S5 (ESI†). Strong emission bands at 481 and 498 nm (Table 1) are observed, respectively, revealing the two compounds to be promising candidates for optoelectronic materials.

3.5. Aggregation induced emission (AIE) properties

Both DETPCZ and DECZDPE are non-emissive or emit weakly when molecularly dissolved but become highly emissive in the aggregated state. To determine the AIE behavior of DETPCZ and DECZDPE, the changes in photoluminescence (PL) intensity as a function of the water-fraction (f_w) in a THF–water mixture were recorded with THF being the good solvent and water acting as a non-solvent. Figs. 2a and 3a depict the PL spectra of DETPCZ and DECZDPE in various THF–water mixtures at an excitation wavelength of 350 nm. DETPCZ displays very weak PL emission in pure THF (the PL peak is at 412 nm). The spectral characteristics of DETPCZ have no significant change for water fractions (f_w) in the range from 0% to 70%. However, upon increasing the water content higher than 70%, the PL peak shifts to 487 nm (Table 1). With the sequential increasing proportion of water, the emission intensity simultaneously becomes stronger. At $f_w = 95\%$, the PL intensity reaches the maximum, with a 114-fold enhancement compared to that in pure THF solution. The plot of $[(I/I_o) - 1]$ against f_w, with I_o and I being the PL intensities without and with water in the THF–water mixtures, visualizes this phenomenon, which is typical for AIE-systems (Fig. 2b). The AIE-behavior of DECZDPE is found to be similar to that of DETPCZ. The PL intensity remains unchanged at low f_w values ($\leq$50%) but begins to increase afterwards (Fig. 3b). At $f_w = 95\%$, strong blue–green fluorescence (500 nm) is recorded reaching a 60-fold increase in intensity in comparison to the pure THF-solution.

In addition, images of DETPCZ and DECZDPE in THF–water mixtures of $f_w = 0$ and 95% are shown as insets in Figs. 2b and 3b, respectively, further demonstrating the AIE-effects. All these results evidently suggest the prominent AIE-characteristics of DETPCZ and DECZDPE, which can be attributed to the RIR process in the aggregate formation. Thus, the radiative relaxation of the excited state becomes more favorable and leads to the strong fluorescence. In terms of the fabrication of optical devices, neither DETPCZ nor DECZDPE need to be doped in order to be emissive in solid-state as both enjoy a high emission intensity.

3.6. Electrochemical properties

The electrochemical properties of DETPCZ and DECZDPE were investigated by cyclic voltammetry (CV) with Ag/AgCl as the reference electrode. The measurements were conducted in a 1.0 mM solution of DETPCZ or DECZDPE in acetonitrile containing 0.10 M tetrabutylammonium perchlorate as the supporting electrolyte under N_2 atmosphere. The CVs of DETPCZ are displayed in Fig. S6a (ESI†). As shown in Fig. S6a†, two reversible oxidation peaks and two reversible reduction peaks are observed within the entire electrochemical window of acetonitrile. The reversible oxidation peaks at 0.54 and 1.17 V are assigned to the oxidation of carbazole and phenylethene, respectively. The reversible reduction peaks at −0.51 and −1.00 V are attributed to the reduction of phenylethene and dimesitylboron, respectively. As evidenced by the CVs in Fig. S6b

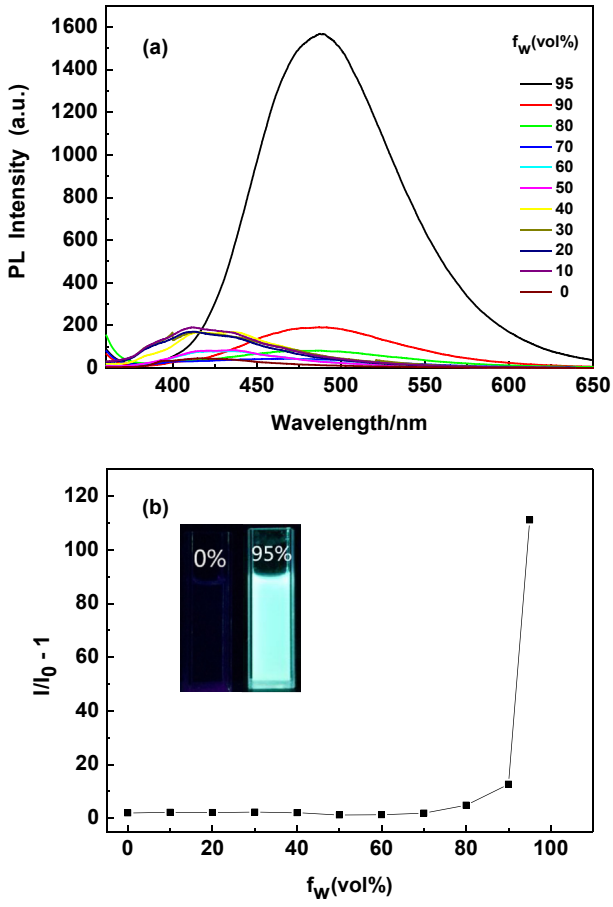

Fig. 2. (a) PL spectra of **DETPCZ** in THF–water mixtures with various water content (excited at 350 nm). (b) Plot of (I/I0) − 1 against water volume fraction (fw), where I0 and I are the PL intensities without and with water in the THF–water mixtures. Inset: photo images of **DETPCZ** in THF–water mixtures with 0% and 95% water fraction.

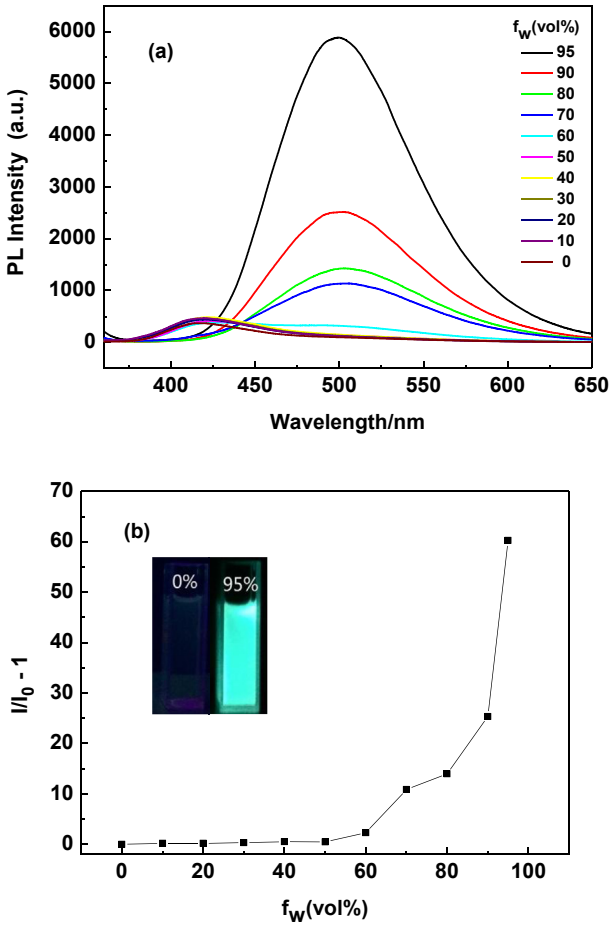

Fig. 3. (a) PL spectra of **DECZDPE** in THF–water mixtures with various water content (excited at 350 nm). (b) Plot of $(I/I_0) - 1$ against water volume fraction (f_w), where I_0 and I are the PL intensities without and with water in the THF–water mixtures. Inset: photo images of **DECZDPE** in THF–water mixtures with 0% and 95% water fraction.

(ESI†), the electrochemical behavior of DECZDPE and DETPCZ are almost similar. The HOMO energy level can be calculated with the empirical equation: HOMO = −(E_{ox} + 4.40) eV, where E_{ox} is the onset oxidation potential [66]. With an E_{ox}-value of 0.50 V, the HOMO energy level of DETPCZ is calculated at −4.90 eV. The E_g is estimated to be 2.92 eV by the absorption edge of the absorption spectrum of DETPCZ. Based on this data, the calculated LUMO energy level of DETPCZ thus amounts to −1.98 eV. The LUMO energy level of DETPCZ is higher than that of *N*,*N*-bis(1-naphthyl)-*N*,*N*-diphenylbenzidine (NPB) (−2.3 eV), which contributes to blocking electron leakage to the anode. The HOMO, LUMO, and E_g of DECZDPE are slightly smaller than those of DETPCZ, which are −5.38, −2.51 eV and 2.87 eV, respectively (Table 1). The HOMO energy level of DECZDPE matches well with that of the common hole-transporting materials, *N*,*N*-bis(1-naphthyl)-*N*,*N*-diphenylbenzidine (NPB) (−5.3 eV), indicating that DECZDPE can play a role as hole-transporting material. Moreover, the CV curves of the compounds remained unchanged under multiple successive potential scans, demonstrating their excellent stability against electrochemical oxidation [67].

3.7. Electroluminescent properties

In order to investigate the EL properties of DETPCZ and DECZDPE, multilayer organic EL devices with the configuration of ITO/HATCN (20 nm)/NPB (40 nm)/DETPCZ (20 nm)/TPBI (40 nm)/LiF (1 nm)/Al (100 nm) (Device I) and ITO/HATCN (20 nm)/NPB (40 nm)/DECZDPE (20 nm)/TPBI (40 nm)/LiF (1 nm)/Al (100 nm) (Device II) were fabricated by vacuum deposition, wherein *N*,*N*-bis(1-naphthyl)-*N*,*N*-diphenylbenzidine (NPB) was used as the hole-transporting layer, 2,2′,2″-(1,3,5-benzinetriyl)tris(1-phenyl-1*H*-benzimidazole) (TPBI) worked as the electron-transporting layer, DETPCZ and DECZDPE functioned as the emitting layer and HATCN served as the hole-injecting layer, respectively. The EL spectra are depicted in Fig. S7 (ESI†). The current density-voltage-luminance and current efficiency-current density curves of the devices are presented in Figs. 4 and 5, respectively and the relevant performance data are summarized in Table 2. As shown in Table 2, the EL spectrum of Device I has a peak maximum of 486 nm which is close to the PL spectrum of the solid thin film of DETPCZ (481 nm) with CIE coordinates of (0.20, 0.28) (Fig. 6). Moreover, Device I exhibits good performance with a turn-on voltage of 4.2 V, a maximum luminance of 13,930 cd m^{-2} at 15 V and a maximum luminescent efficiency of 4.74 cd A^{-1} at 5.4 V. Compared with Device I, the EL spectrum of Device II exhibits a bright blue–green emission with a maximum at 512 nm and CIE coordinates of (0.23, 0.41) (Fig. 6), which is red-shifted about 14 nm in contrast with its PL emission in solid film (λ_{em} 498 nm). The turn-on voltage, maximum luminance and maximum luminescent efficiency of Device II are 4.4 V, 15,780 cd m^{-2} and 6.90 cd A^{-1}, respectively. The two devices have similarly high EL performance when compared with those devices fabricated by some other AIE luminogens [54,57,59]. All these attributes make DETPCZ and DECZDPE

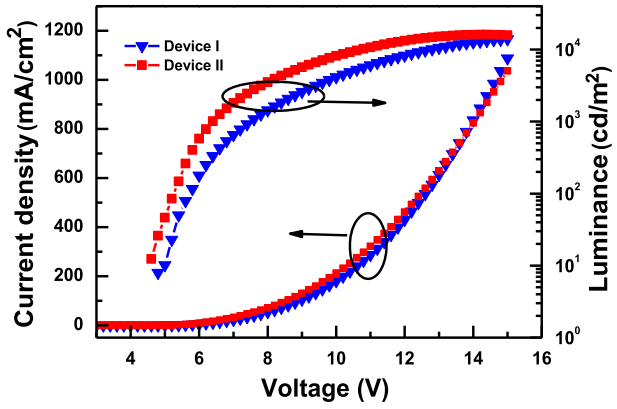

Fig. 4. Current density–voltage–luminance curves of **Device I** and **II**.

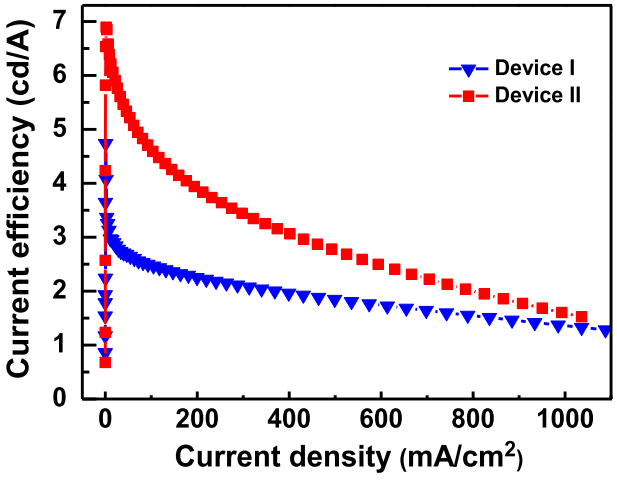

Fig. 5. Current efficiency–current density curves of **Device I** and **II**.

promising candidates for innovative applications in OLEDs systems due to their high thermal stability, efficient and improved solid-state emissions, and excellent electroluminescence properties.

4. Conclusions

In summary, two novel AIE-luminogens, DETPCZ and DECZDPE, have been successfully synthesized through a innovative integration of phenylethylene, carbazole and dimesitylboron groups, and characterized by elemental analysis, ^{1}H NMR, ^{13}C NMR, IR and MS. The thermal, electrochemical and photophysical properties of DETPCZ and DECZDPE were studied by combination of experimental and theoretical methods. Our results show that DETPCZ and DECZDPE enjoy excellent thermal stability (T_d up to 254 °C) and exhibit high electrochemical stability and solid-state emissions.

Table 2
Electroluminescent characteristics of **Devices I** and **II**.

Device	V_{on}[a] (V)	L_{max}[b] (cd/m^2)	CE_{max}[c] (cd/A)	λ_{EL}[d] (nm)	CIE (x, y)
I	4.2	13,930	4.74	486	(0.20, 0.28)
II	4.4	15,780	6.90	512	(0.23, 0.41)

[a] Turn on voltage at a brightness of 1 cd/m^2.
[b] Maximum luminance.
[c] Maximum current efficiency.
[d] Electroluminescence peak.

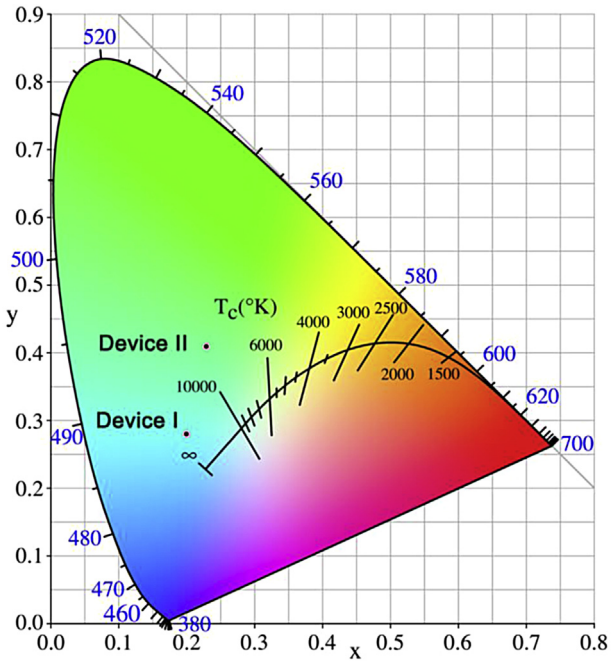

Fig. 6. Commission Internationale de l'Eclairage (CIE) chromaticity coordinates of **Device I** and **II**.

Furthermore, the multi-layer EL devices using DETPCZ and/or DECZDPE as light-emitting layer were fabricated, which yielded sky blue and blue–green EL with maximum luminance efficiency and maximum luminance up to 6.90 cd A^{-1} and 15,780 cd m^{-2} at CIE chromaticity coordinates of (0.20, 0.28) and (0.23, 0.41), respectively. Our research strategy provides a new way for the creation and application of novel AIE-luminophores.

Acknowledgments

This work was supported by the Science and Technology Innovation Project of Shanxi Province (No. 2014101011); Natural Science Foundation of Shanxi Province (No. 2014011003); State Key Laboratory of Structural Chemistry, Fujian Institute of Research on the Structure of Matter, Chinese Academy of Sciences (No. 20140016); Beijing National Laboratory for Molecular Sciences (No. BNLMS 2013031); Scientific and Technological Innovation Programs of Higher Education Institutions in Shanxi Province (No. 2014109 and 2012005); National Natural Science Foundation of China (No. 61405089); The Innovation of Science and Technology Committee of Shenzhen (No. JCYJ20140417105742713) and Fund of Key Laboratory of Optoelectronic Materials Chemistry and Physics, Chinese Academy of Sciences (No. 2008DP173016). The authors express their sincere thanks to the Advanced Computing Facilities of the Supercomputing Centre of Computer Network Information Centre of Chinese Academy of Sciences for all the theoretical calculations.

Appendix A. Supplementary data

Supplementary data related to this article can be found at http://dx.doi.org/10.1016/j.dyepig.2016.01.028.

References

[1] Burroughes JH, Bradley DDC, Brown AR, Marks RN, Mackay K, Friend RH, et al. Light-emitting diodes based on conjugated polymers. Nature 1990;347:539–41.

[2] Hung LS, Chen CH. Recent progress of molecular organic electroluminescent materials and devices. Mater Sci Eng R 2002;39:143–222.
[3] Mitschke U, Bäuerle P. The electroluminescence of organic materials. J Mater Chem 2000;10:1471–507.
[4] Shirota Y. Organic materials for electronic and optoelectronic devices. J Mater Chem 2000;10:1–25.
[5] Lamansky S, Djurovich P, Murphy D, Abdel-Razzaq F, Lee H-E, Adachi C, et al. Highly phosphorescent bis-cyclometalated iridium complexes: synthesis, photophysical characterization, and use in organic light emitting diodes. J Am Chem Soc 2001;123:4304–12.
[6] Kim DH, Cho NS, Oh H-Y, Yang JH, Jeon WS, Park JS, et al. Highly efficient red phosphorescent dopants in organic light-emitting devices. Adv Mater 2011;23:2721–6.
[7] Zhu MR, Yang CL. Blue fluorescent emitters: design tactics and applications in organic light-emitting diodes. Chem Soc Rev 2013;42:4963–76.
[8] Fisher AL, Linton KE, Kamtekar KT, Pearson C, Bryce MR, Petty MC. Efficient deep-blue electroluminescence from an ambipolar fluorescent emitter in a single-active-layer device. Chem Mater 2011;23:1640–2.
[9] Sax S, Rugen-Penkalla N, Neuhold A, Schuh S, Zojer E, List EJW, et al. Efficient blue-light-emitting polymer heterostructure devices: the fabrication of multilayer structures from orthogonal solvents. Adv Mater 2010;22:2087–91.
[10] Wu K-C, Ku P-J, Lin C-S, Shih H-T, Wu F-I, Huang M-J, et al. The photophysical properties of dipyrenylbenzenes and their application as exceedingly efficient blue emitters for electroluminescent devices. Adv Funct Mater 2008;18:67–75.
[11] Cho I, Kim SH, Kim JH, Park S, Park SY. Highly efficient and stable deep-blue emitting anthracene-derived molecular glass for versatile types of non-doped OLED applications. J Mater Chem 2012;22:123–9.
[12] Kim SH, Cho I, Sim MK, Park S, Park SY. Highly efficient deep-blue emitting organic light emitting diode based on the multifunctional fluorescent molecule comprising covalently bonded carbazole and anthracene moieties. J Mater Chem 2011;21:9139–48.
[13] Park H, Lee J, Kang I, Chu HY, Lee J-I, Kwon S-K, et al. Highly rigid and twisted anthracene derivatives: a strategy for deep blue OLED materials with theoretical limit efficiency. J Mater Chem 2012;22:2695–700.
[14] Leung LM, Lo WY, So SK, Lee KM, Choi WK. A high-efficiency blue emitter for small molecule-based organic light-emitting diode. J Am Chem Soc 2000;122:5640–1.
[15] Tseng RJ, Chiechi RC, Wudl F, Yang Y. Highly efficient 7,8,10-triphenylfluoranthene-doped blue organic light-emitting diodes for display application. Appl Phys Lett 2006;88:093512-1–093512-3.
[16] Saragi TPI, Spehr T, Siebert A, Fuhrmann-Lieker T, Salbeck J. Spiro compounds for organic optoelectronics. Chem Rev 2007;107:1011–65.
[17] Lyu Y-Y, Kwak J, Kwon O, Lee S-H, Kim D, Lee C, et al. Silicon-cored anthracene derivatives as host materials for highly efficient blue organic light-emitting devices. Adv Mater 2008;20:2720–9.
[18] Kamtekar KT, Monkman AP, Bryce MR. Recent advances in white organic light-emitting materials and devices (WOLEDs). Adv Mater 2010;22:572–82.
[19] Grimsdale AC, Chan KL, Martin RE, Jokisz PG, Holmes AB. Synthesis of light-emitting conjugated polymers for applications in electroluminescent devices. Chem Rev 2009;109:897–1091.
[20] Thomas III SW, Joly GD, Swager TM. Chemical sensors based on amplifying fluorescent conjugated polymers. Chem Rev 2007;107:1339–86.
[21] Liu JZ, Lam JWY, Tang BZ. Acetylenic polymers: syntheses, structures, and functions. Chem Rev 2009;109:5799–867.
[22] Pu K-Y, Liu B. Conjugated polyelectrolytes as light-up macromolecular probes for heparin sensing. Adv Funct Mater 2009;19:277–84.
[23] Luo JD, Xie ZL, Lam JWY, Cheng L, Chen HY, Qiu CF, et al. Aggregation-induced emission of 1-methyl-1,2,3,4,5-pentaphenylsilole. Chem Commun 2001:1740–1.
[24] Chen JW, Xu B, Ouyang XY, Tang BZ, Cao Y. Aggregation-induced emission of cis,cis-1,2,3,4-tetraphenylbutadiene from restricted intramolecular rotation. J Phys Chem A 2004;108:7522–6.
[25] Li Z, Dong YQ, Mi BX, Tang YH, Häussler M, Tong H, et al. Structural control of the photoluminescence of silole regioisomers and their utility as sensitive regiodiscriminating chemosensors and efficient electroluminescent materials. J Phys Chem B 2005;109:10061–6.
[26] Ren Y, Lam JWY, Dong YQ, Tang BZ, Wong KS. Enhanced emission efficiency and excited state lifetime due to restricted intramolecular motion in silole aggregates. J Phys Chem B 2005;109:1135–40.
[27] Hong YN, Lam JWY, Tang BZ. Aggregation-induced emission: phenomenon, mechanism and applications. Chem Commun 2009:4332–53.
[28] Hong YN, Lam JWY, Tang BZ. Aggregation-induced emission. Chem Soc Rev 2011;40:5361–88.
[29] Chen L, Jiang YB, Nie H, Lu P, Sung HHY, Williams ID, et al. Creation of bifunctional materials: improve electron-transporting ability of light emitters based on AIE-active 2,3,4,5-tetraphenylsiloles. Adv Funct Mater 2014;24:3621–30.
[30] Scalise RE, Caradonna PA, Tracy HJ, Mullin JL, Keirstead AE. 1,1-Dimethyl-2,3,4,5-tetraphenylsilole as a molecular rotor probe to investigate the microviscosity of imidazolium ionic liquids. J Inorg Organomet Polym Mater 2014;24:431–41.
[31] Mei J, Wang J, Sun JZ, Zhao H, Yuan WZ, Deng CM, et al. Siloles symmetrically substituted on their 2,5-positions with electron-accepting and donating moieties: facile synthesis, aggregation-enhanced emission, solvatochromism, and device application. Chem Sci 2012;3:549–58.
[32] Zhou J, He BR, Chen B, Lu P, Sung HHY, Williams ID, et al. Deep blue fluorescent 2,5-bis(phenylsilyl)-substituted 3,4-diphenylsiloles: synthesis, structure and aggregation-induced emission. Dyes Pigments 2013;99:520–5.
[33] Zhao ZJ, Lam JWY, Tang BZ. Tetraphenylethene: a versatile AIE building block for the construction of efficient luminescent materials for organic light-emitting diodes. J Mater Chem 2012;22:23726–40.
[34] Huang J, Sun N, Dong YQ, Tang RL, Lu P, Cai P, et al. Similar or totally different: the control of conjugation degree through minor structural modifications, and deep-blue aggregation-induced emission luminogens for non-doped OLEDs. Adv Funct Mater 2013;23:2329–37.
[35] Gu XG, Yao JJ, Zhang GX, Zhang C, Yan YL, Zhao YS, et al. New electron-donor/acceptor-substituted tetraphenylethylenes: aggregation-induced emission with tunable emission color and optical-waveguide behavior. Chem Asian J 2013;8:2362–9.
[36] Dong WY, Fei T, Palma-Cando A, Scherf U. Aggregation induced emission and amplified explosive detection of tetraphenylethylene-substituted polycarbazoles. Polym Chem 2014;5:4048–53.
[37] Luo M, Zhou X, Chi ZG, Liu SW, Zhang Y, Xu JR. Fluorescence-enhanced organogelators with mesomorphic and piezofluorochromic properties based on tetraphenylethylene and gallic acid derivatives. Dyes Pigments 2014;101:74–84.
[38] He BR, Chang ZF, Jiang YB, Xu XF, Lu P, Kwok HS, et al. Piezochromic luminescent and electroluminescent materials comprised of tetraphenylethene plus spirobifluorene or 9,9-diphenylfluorene. Dyes Pigments 2014;106:87–93.
[39] Zhan XJ, Yang M, Yuan L, Gong YB, Xie YJ, Peng Q, et al. Prying into the limit of CIE value for TPE-based blue AIEgens in organic light-emitting diodes. Dyes Pigments 2016;128: 60–67.
[40] Zhang XQ, Chi ZG, Xu BJ, Jiang L, Zhou X, Zhang Y, et al. Multifunctional organic fluorescent materials derived from 9,10-distyrylanthracene with alkoxyl endgroups of various lengths. Chem Commun 2012;48:10895–7.
[41] He JT, Xu B, Chen FP, Xia HJ, Li KP, Ye L, et al. Aggregation-induced emission in the crystals of 9,10-distyrylanthracene derivatives: the essential role of restricted intramolecular torsion. J Phys Chem C 2009;113:9892–9.
[42] Yang ZY, Chi ZG, Yu T, Zhang XQ, Chen MN, Xu BJ, et al. Triphenylethylene carbazole derivatives as a new class of AIE materials with strong blue light emission and high glass transition temperature. J Mater Chem 2009;19:5541–6.
[43] Zhang XQ, Chi ZG, Li HY, Xu BJ, Li XF, Liu SW, et al. Synthesis and properties of novel aggregation-induced emission compounds with combined tetraphenylethylene and dicarbazolyl triphenylethylene moieties. J Mater Chem 2011;21:1788–96.
[44] Zhang XQ, Chi ZG, Xu BJ, Chen CJ, Zhou X, Zhang Y, et al. End-group effects of piezofluorochromic aggregation-induced enhanced emission compounds containing distyrylanthracene. J Mater Chem 2012;22:18505–13.
[45] Liu C, He W, Shi G, Luo HY, Zhang S, Chi ZG. Synthesis and properties of a new class of aggregation-induced enhanced emission compounds: intense blue light emitting triphenylethylene derivatives. Dyes Pigments 2015;112:154–61.
[46] Han T, Zhang YJ, Feng X, Lin ZG, Tong B, Shi JB, et al. Reversible and hydrogen bonding-assisted piezochromic luminescence for solid-state tetraaryl-buta-1,3-diene. Chem Commun 2013;49:7049–51.
[47] Guo YX, Feng X, Han TY, Wang S, Lin ZG, Dong YP, et al. Tuning the luminescence of metal–organic frameworks for detection of energetic heterocyclic compounds. J Am Chem Soc 2014;136:15485–8.
[48] Qin W, Yang ZY, Jiang YB, Lam JWY, Liang GD, Kwok HS, et al. Construction of efficient deep blue aggregation-induced emission luminogen from triphenylethene for nondoped organic light-emitting diodes. Chem Mater 2015;27:3892–901.
[49] Yang ZY, Qin W, Lam JWY, Chen SJ, Sung HHY, Williams ID, et al. Fluorescent pH sensor constructed from a heteroatom-containing luminogen with tunable AIE and ICT characteristics. Chem Sci 2013;4:3725–30.
[50] Yang ZY, Chi ZG, Xu BJ, Li HY, Zhang XQ, Li XF, et al. High-T_g carbazole derivatives as a new class of aggregation-induced emission enhancement materials. J Mater Chem 2010;20:7352–9.
[51] Zhang XQ, Chi ZG, Xu BJ, Li HY, Yang ZY, Li XF, et al. Synthesis of blue light emitting bis(triphenylethylene) derivatives: a case of aggregation-induced emission enhancement. Dyes Pigments 2011;89:56–62.
[52] Zhang XQ, Yang ZY, Chi ZG, Chen MN, Xu BJ, Wang CC, et al. A multi-sensing fluorescent compound derived from cyanoacrylic acid. J Mater Chem 2010;20:292–8.
[53] Xu BJ, Chi ZG, Li XF, Li HY, Zhou W, Zhang XQ, et al. Synthesis and properties of diphenylcarbazole triphenylethylene derivatives with aggregation-induced emission, blue light emission and high thermal stability. J Fluoresc 2011;21:433–41.
[54] Chan CYK, Lam JWY, Zhao ZJ, Chen SM, Lu P, Sung HHY, et al. Aggregation-induced emission, mechanochromism and blue electroluminescence of carbazole and triphenylamine-substituted ethenes. J Mater Chem C 2014;2:4320–7.
[55] Zhou J, Chang ZF, Jiang YB, He BR, Du M, Lu P, et al. From tetraphenylethene to tetranaphthylethene: structural evolution in AIE luminogen continues. Chem Commun 2013;49:2491–3.

[56] Huang J, Yang X, Wang JY, Zhong C, Wang L, Qin JG, et al. New tetraphenylethene-based efficient blue luminophors: aggregation induced emission and partially controllable emitting color. J Mater Chem 2012;22:2478–84.
[57] Gong WL, Wang B, Aldred MP, Li C, Zhang GF, Chen T, et al. Tetraphenylethene-decorated carbazoles: synthesis, aggregation-induced emission, photooxidation and electroluminescence. J Mater Chem C 2014;2:7001–12.
[58] Zhao ZJ, Chan CYK, Chen SM, Deng CM, Lam JWY, Jim CKW, et al. Using tetraphenylethene and carbazole to create efficient luminophores with aggregation-induced emission, high thermal stability, and good hole-transporting property. J Mater Chem 2012;22:4527–34.
[59] Liu Y, Ye X, Liu GF, Lv Y, Zhang XY, Chen SM, et al. Structural features and optical properties of a carbazole-containing ethene as a highly emissive organic solid. J Mater Chem C 2014;2:1004–9.
[60] Zhao CH, Wakamiya A, Inukai Y, Yamaguchi S. Highly emissive organic solids containing 2,5-diboryl-1,4-phenylene unit. J Am Chem Soc 2006;128:15934–5.
[61] Entwistle CD, Marder TB. Applications of three-coordinate organoboron compounds and polymers in optoelectronics. Chem Mater 2004;16:4574–85.
[62] Hohenberg P, Kohn W. Phys Rev B Solid State 1964;136:864–71.
[63] Kohn W, Sham LJ. Phys Rev A At Mol Opt Phys 1965;140:1133–8.
[64] Foresman JB, Gordon MH, Pople JA, Frisch MJ. Toward a systematic molecular orbital theory for excited states. J Phys Chem 1992;96:135–49.
[65] Frisch MJ, Trucks GW, Schlegel HB, Scuseria GE, Robb MA, Cheeseman JR, et al. GAUSSIAN 03 (Revision B.05). Pittsburgh, PA: Gaussian, Inc.; 2003.
[66] Brédas JL, Silbey R, Boudreaux DS, Chance RR. Chain-length dependence of electronic and electrochemical properties of conjugated systems: polyacetylene, polyphenylene, polythiophene, and polypyrrole. J Am Chem Soc 1983;105:6555–9.
[67] Promaraka V, Ruchirawat S. Synthesis and properties of N-carbazole end-capped conjugated molecules. Tetrahedron 2007;63:1602–9.